RSC Advances

This is an *Accepted Manuscript*, which has been through the Royal Society of Chemistry peer review process and has been accepted for publication.

Accepted Manuscripts are published online shortly after acceptance, before technical editing, formatting and proof reading. Using this free service, authors can make their results available to the community, in citable form, before we publish the edited article. This *Accepted Manuscript* will be replaced by the edited, formatted and paginated article as soon as this is available.

You can find more information about *Accepted Manuscripts* in the Information for Authors.

Please note that technical editing may introduce minor changes to the text and/or graphics, which may alter content. The journal's standard Terms & Conditions and the Ethical guidelines still apply. In no event shall the Royal Society of Chemistry be held responsible for any errors or omissions in this *Accepted Manuscript* or any consequences arising from the use of any information it contains.

ROYAL SOCIETY OF CHEMISTRY

www.rsc.org/advances

TOC Figure

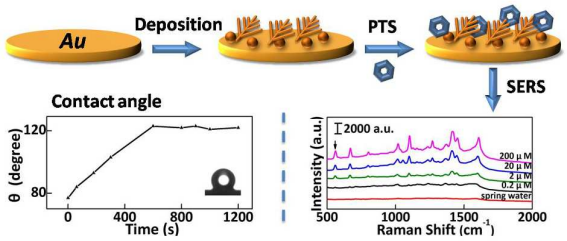

The hydrophobic gold nanostructures were used for direct SERS detection of PTS with high sensitivity.

RSC Advances Accepted Manuscript

Cite this: DOI: 10.1039/c0xx00000x

www.rsc.org/xxxxxx

ARTICLE TYPE

Hydrophobic gold nanostructures via electrochemical deposition for sensitive SERS detection of persistent toxic substances

Lixiao Jing, Yu-e Shi, Jingcheng Cui, Xiaoli Zhang,* and Jinhua Zhan*

Received (in XXX, XXX) Xth XXXXXXXXX 20XX, Accepted Xth XXXXXXXXX 20XX

DOI: 10.1039/b000000x

The Persistent toxic substances (PTS), pollutants that have environmental persistence and toxic effects such as carcinogenicity and endocrine disruption, are generally detected by the chromatographic method. In this work, hydrophobic gold nanostructures were fabricated via simple electrochemical deposition and could be used for direct SERS detection of PTS with a portable Raman spectrometer. The obtained hydrophobic substrates free from modification show high affinity towards PTS, such as polycyclic aromatic hydrocarbons (PAHs), polybrominated diphenyl ethers (PBDEs) and polychlorinated biphenyls (PCBs). According to the Cassie equation, wetting property of the surface changed from hydrophilic to hydrophobic with the contact angle changed from 77° to 123°, increasing the deposition time. The SERS signals collected on sixteen randomly selected points show that the relative standard deviation of the SERS intensity is 9.0%, indicating the substrate had good uniformity. Quantitative SERS detection of PTS was achieved, as the log-log plot of SERS intensity to PTS concentration exhibited a good linear relationship in view of the Freundlich equation. Quantitative analysis of fluoranthene, BDE-15 and PCB-15 was accomplished in the concentration range of 0.02-200 μM, 0.02-200 μM, 0.04-440 μM, with the detection limits of 6.7 nM, 2.6 nM and 5.3 nM, respectively. The effective SERS substrates provide a rapid and sensitive platform for trace level detection of hydrophobic contaminants in the environment.

Introduction

Persistent toxic substances (PTS), contaminants that are implicated in environmental persistence, carcinogenesis and endocrine disruption, have concerned the United Nations Environment Programme (UNEP).[1-3] A list of PTS comprising 27 species of toxic chemical contaminants have been established by UNEP. Polycyclic aromatic hydrocarbons (PAHs), polybrominated diphenyl ethers (PBDEs) and polychlorinated biphenyls (PCBs), representatives of these various contaminants in the environment, are contained in the list due to their chemical inertness and lipophilicity.[4] As the main sources of the three typical PTS, incomplete combustion of gasoline, addition of brominated flame retardants and usage of insulating fluids in heavy-duty electrical equipment, have been confirmed to take responsibility for the generation of PAHs, PBDEs, PCBs, respectively. They are widely found in waste water and underground water which can accumulate from low level to harmful concentration.[4,5] In order to identify and monitor PTS in environmental media,[6-8] several analytical methods including gas chromatography (GC) coupled with mass spectrometry or electron capture detectors (GC-MS or GC-ECD) and high-performance liquid chromatography (HPLC) coupled with UV or MS have been developed.[8-13]

Surface-enhanced Raman spectroscopy (SERS) has been developed into a powerful technique for environmental monitoring, chemical analysis and biomedical research due to its high sensitivity, selectivity and speed.[14-22] In SERS measurements, the Raman signals of the adsorbed resonant molecules can be amplified as high as 14 orders.[23, 24] Generally, the Raman enhancement can be attributed to two mechanisms: the electromagnetic (EM) mechanism associated with the localized surface plasmon resonance (LSPR), and the chemical mechanism (CM) arising from the special chemical interactions between the analytes and the substrate. The EM enhancement related to the nanostructure properties could play a major role in SERS process.[25,26] Up to now, various methods such as wet-chemical route,[27] seeded growth,[28] hydrothermal reduction,[29] templating,[30] electrodeposition[31, 32] have been employed to obtain the noble metal nanostructures as effective SERS substrate. Large SERS signals could be obtained when the analytes are very close to the substrate surface and the SERS signals decays exponentially accordingly to the distance from SERS substrate.[33] Therefore, the Raman signals of the analytes with specific functional groups (such as thiol, carboxylic acid, amine, etc.) that act as an anchor to the substrate surface could be easily enhanced. As for the chemical inertial contaminants like PAHs, PBDEs and PCBs with low affinity to pristine noble metal surface, surface functionalization procedures are generally needed to bring target molecule to the SERS-effective LSPR field. Silver functionalized by cyclodextrin derivatives have been used as SERS-active substrates for effective capture of analyte molecule into its hydrophobic cavity with host-guest interactions.[34-36] Other SERS

RSC Advances Accepted Manuscript

substrates, functionalized by propanethiol,[37] 1-hexanethiol,[38,39] were developed to bring analyte molecule to alkanethiol self-assembled monolayer with hydrophobic interactions. It was also demonstrated that Raman signals decreased as the chain length increased.[39]

Herein, hydrophobic gold nanostructures have been fabricated via a facile potentiostatic electrodeposition method as SERS substrates for direct detection of PTS with a portable Raman spectrometer. The hydrophobic gold nanostructures with a "clean" surface could be used direct without further surface modification. Due to the hydrophobic property, the as-obtained nanostructures show high affinity towards PAHs, PBDEs and PCBs and could be ideal candidates of SERS substrate for rapid trace level detection.

Experimental section

Chemicals

All the chemicals were analytical reagent grade and used as purchased without further purification. *p*-Aminothiophenol (PATP) was purchased from Acros Organics. Ethanol was obtained from Sinopharm Chemical Reagent Co. Ltd. (Shanghai, China). $HAuCl_4$ was purchased from Shanghai Chemical Reagents Co. Ltd. (Shanghai, China). Fluoranthene was purchased from Tokyo Chemical Industry. 4, 4′-Dibromodiphenyl ether (BDE-15) was purchased from Aldrich. 4, 4′-Dichlorobiphenyl (PCB-15) was purchased from J & K Chemical Co. Ltd. Ultrapure water (18.2 MΩ cm^{-1}) was used throughout the experiments.

Apparatus

The Raman measurements were recorded on a portable Raman spectrometer (Ocean Optics QE65000). The electrochemical experiments were carried out on a CHI-660C electrochemical analyzer (Shanghai Chenhua, China). A conventional three-electrode system was used in this work, including an Ag/AgCl electrode (saturated KCl) as the reference electrode, a platinum wire as the counter electrode and a bare gold electrode (3 mm diameter) as the working electrode. All the potentials were reported versus the Ag/AgCl (saturated KCl) reference electrode. Scanning electron microscope (SEM) image and energy dispersive spectroscopy (EDS) analysis were recorded by JEOL JSM-6700F microscope with an EDS system (Japan).

Preparation of the hydrophobic gold nanostructures

The bare gold electrode was successively polished with 0.50 μm and 0.05 μm alumina slurry and ultrasonicated in absolute ethanol and doubly distilled water in turn for 10 min. Then the gold electrode was immersed into 0.1 M KNO_3 containing 0.4 g L^{-1} $HAuCl_4$, and the electrodeposition process was conducted at -0.6 V for 600 s. The as-obtained gold nanostructures modified electrode was taken out, cleaned, and dried with high-purity flowing nitrogen. Moreover, the wetting property of the surface was studied by contact angle measurement (Kruss DSA10, Germany). Water droplets (2 μL) were dropped carefully on to the electrode surface, and the average value of three measurements was collected and adopted as the contact angle.

SERS measurements

Stock solutions of PTS were prepared by dissolving them in ethanol at an initial concentration of 1 mM, and diluted to the desired concentration with water. The gold nanostructures modified gold electrode was used as substrates for SERS detection. For checking SERS performance, the substrates were immersed in PTS solutions for 10 min with stirring at room temperature. SERS signals from three different spots on substrates were measured. All the measurements were conducted after drying the substrates at ambient environment. The excitation wavelength was 785 nm and the laser power was 440 mW. Integration time was 1 s.

Results and discussion

Effects of the deposition conditions on morphology and SERS intensity

The morphology of deposited gold nanostructures could be controlled to some extent through choosing deposition conditions, such as deposition time, deposition potential and so on. Fig. 1 illustrates SEM images of gold nanostructures electrodeposited on gold electrode via different deposition time under constant potential of -0.6 V from the solution containing 0.4 g L^{-1} $HAuCl_4$. As shown in Fig. 1A, visible gold nanoparticles were first generated within just 180s of deposition. Increasing the electrodeposition time, gold nanoparticles with rough surfaces augmented and subsequent growth preferentially occurred on the preformed gold nanoparticles, finally leading to the formation of gold dendrites (Fig. 1). Higher-magnification images (insets in Fig. 1) revealed that the branches were larger, coarser, and denser. The chemical composition of the gold nanostructures was determined by energy-dispersive spectrometer (EDS) analysis. The EDS spectrum showed only Au signals (see Fig. S1), indicating that these nanostructures consisted of pure Au. With prolonged the electrodeposition time, the morphology of the gold deposits changed, and the dendritic structures were obtained gradually. As a result, the surface roughness became larger with the increase of the electrodeposition time. It was demonstrated that electro-deposition time remarkably influenced the morphologies of the gold nanostructures, which would resultantly have dramatically different enhancement on SERS.

To assess the SERS performance of the obtained gold nanostructures, we used *p*-aminothiophenol (PATP) and fluoranthene as probe molecules to study the impact of the electrodeposition time on the SERS activity of the as-fabricated substrates. Fig. 2 depicts the SERS intensities of (a) fluoranthene at 559 cm^{-1}, (b) PATP at 1080 cm^{-1} on the prepared gold nanostructures substrates, versus the electrodeposition time. As can be seen, the SERS intensities of both fluoranthene and PATP increased gradually with the electrodeposition time. When the deposition time was prolonged to 600 s, the SERS intensities of both reached a constant value. As shown in Fig. S2, the as-obtained gold nanostructures exhibited excellent SERS ability for PATP and fluoranthene. In addition, the morphology and SERS activity of the gold nanostructures was found to be potential controlled (see Fig. S3-S4). Gold nanostructures grew densely under potentials of -0.2 V and -1.0 V, and most of the structures grown were uniform spherical particles. It was found that an optimal electrodeposition potential was -0.6 V, in which the as-

RSC Advances Accepted Manuscript

This journal is © The Royal Society of Chemistry [year]

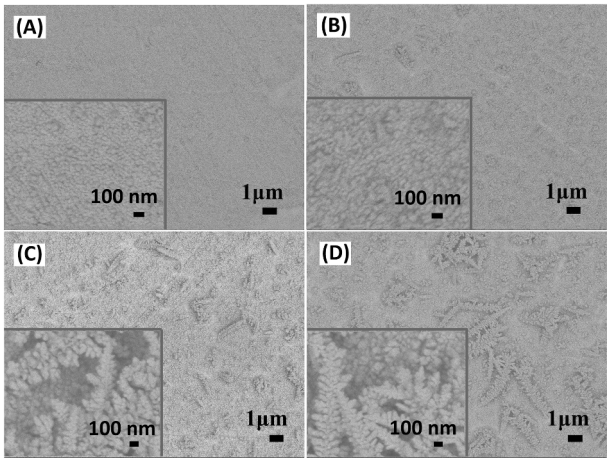

Fig. 1 SEM images of gold nanostructures (insets show high-resolution images) formed on a gold electrode by electrochemical deposition at -0.6 V (vs Ag/AgCl) in the solution of 0.1 M KNO_3 containing 0.4 g L^{-1} $HAuCl_4$. Deposition time is (A) 180 s, (B) 300 s, (C) 600s, (D) 900s.

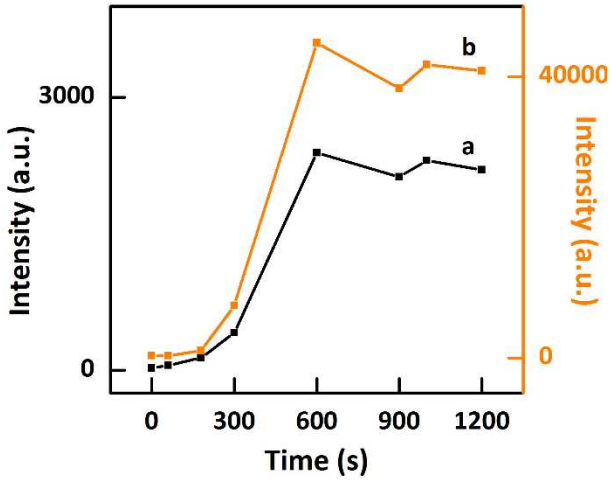

Fig. 2 Diagram of SERS intensities of (a) fluoranthene at 559 cm^{-1}, (b) PATP at 1080 cm^{-1} versus time of electrochemical deposition at -0.6 V (vs Ag/AgCl).

prepared gold nanostructures possessed the excellent enhancement toward SERS. Meanwhile, the gold substrate consisted of a large quantity of dendritic gold nanostructures. Comparing the SERS activities of substrates with different surface roughness, it was noted that the SERS intensity depended on the amount of molecules adsorbed on the surfaces, which could be affected by the roughness of each surface. It was suggested that the high SERS activity could be related to the "clean" surface and morphology of the gold nanostructures, providing a large surface area and numerous "hot spots". Additionally, the enhancement factor (EF) was calculated using $(I_{SERS}/I_{NR}) \times (C_{NR}/C_{SERS})$.[38] I_{SERS} represented the SERS intensity of the most obvious band for analytes, and I_{NR} represented the normal Raman intensity of analytes solution. Meanwhile, C_{NR} and C_{SERS} represented the concentrations of analytes solution. The EF value for fluoranthene and PATP was 1.5×10^4 and 2.6×10^5, respectively, indicating the as-prepared gold nanostructures had good sensitivity as SERS supports. Molecules that chemically adsorbed onto the nanostructure show not only electromagnetic enhancement (EM) but also chemical enhancement (CE).

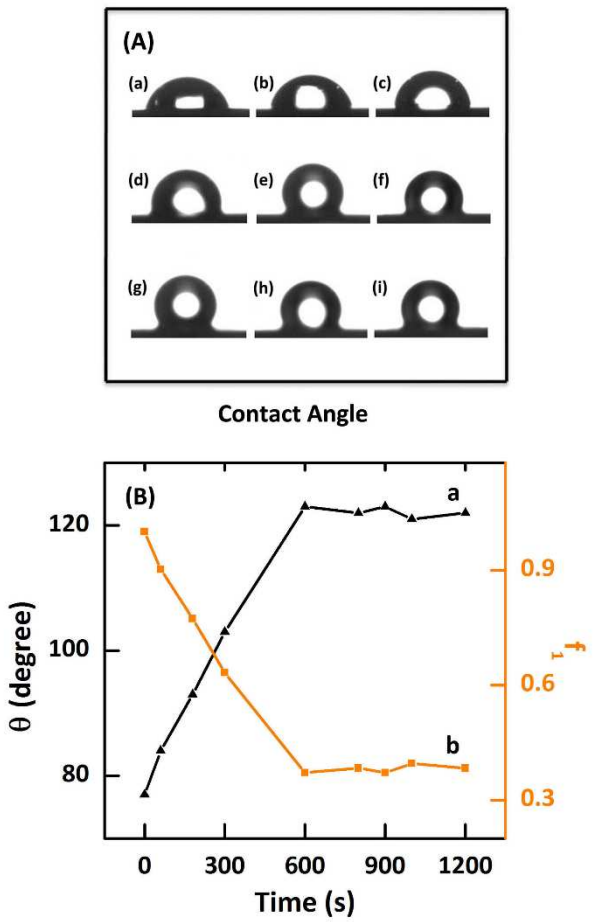

Fig. 3 (A) Contact angle measurements of a water droplet (2μL) on gold nanostructures by electrochemical deposition at -0.6 V (vs Ag/AgCl). Contact angle is (a) 77°, (b) 84°, (c) 93°, (d)103°, (e) 123°, (f) 122°, (g) 123°, (h) 121°, (i) 122° and (B) (a) Dynamic water contact angle measurements and (b) fractional interfacial areas of the air on the surface of gold nanostructures as a function of the duration of electrochemical deposition at -0.6 V (vs Ag/AgCl).

Contrary to EM, CE is analyte-dependent, which is usually magnified by 1–2 orders.[25]

Static contact angle

The contact angle of the gold nanostructures surface was measured to investigate the hydrophilic/hydrophobic features, as shown in Fig. 3A. It was noted that the bare gold electrode was a relatively hydrophilic interface with a contact angle of about 77°. As can been seen from Fig. 3B, the contact angles of the surface increased gradually with the increase of the electrodeposition time, indicating the wettability changed from hydrophilic to hydrophobic. For 180 s electrodeposition time, the obtained gold nanostructures had exhibited hydrophobicity with a contact angle of 93°. After 600 s, the contact angle reached a constant value, as high as 123°. These results revealed that the gold nanostructures were responsible for the hydrophobicity. To understand the hydrophobicity of the surface of the modified electrode, contact angle was described according to the Cassie equation: $\cos\theta_r = f_1\cos\theta - f_2$. θ_r (123°) and θ（77°）are the contact angles on the gold nanostructures with a rough surface and on the bare gold electrode with a smooth gold surface, respectively; f_1 and f_2 are

RSC Advances Accepted Manuscript

the fractional interfacial areas of the gold nanostructures and of the air in the interspaces among the gold nanostructures, respectively (i.e. $f_1+f_2=1$). According to the Cassie equation, the contact angle of the rough surface (θ_r) increases with the fraction of air (f_2). The f_2 value of the rough surface with gold nanostructures is estimated to be 0.63. The hydrophobicity of the as-obtained substrate may be due to the fraction of air in the surface. In order to better understand the change of the contact angle, the fractional of the gold nanostructures (f_1), which is related to the surface roughness, is deduced by mathematics: $f_1=(\cos\theta_r+1)/(\cos\theta_1+1)$. Here, θ_1 is the contact angles on the bare gold electrode with a smooth gold surface. Therefore, the value of f_1 can be calculated from the equation. As shown in Fig. 3B, f_1 decreased gradually with the increase of the electrodeposition time. It was indicated that the surface roughness became higher, which was consistent with the SEM images shown in Fig. 1. The rough nanostructures with hydrophobic surfaces are advantageous for the approach of the hydrophobic probe due to hydrophobic interactions, which may be beneficial to the SERS detection for PTS, such as PAHs, PBDEs and PCBs.

SERS performance of the substrate

The stability and uniformity of SERS intensities are very important aspects for the application of SERS-active substrates in analytical fields. As was well known, stability was a parameter determining the practical utility of SERS-active substrates. A series of Raman spectra were taken in 180 s with an interval time of 5 s. The integration time of each Raman spectrum was 1 s. Fig. 4A demonstrates the temporal stability of the gold nanostructures.

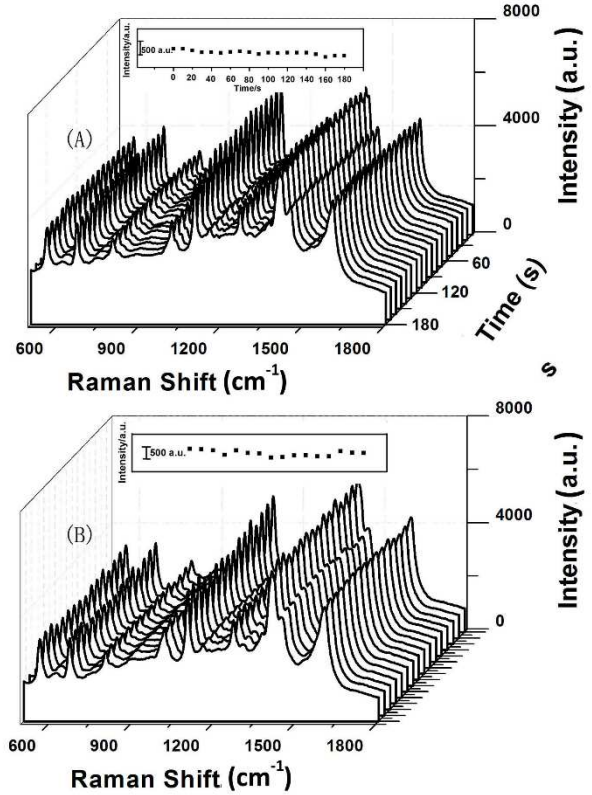

Fig. 4 (A) The temporal stability and (B) the uniformity of the substrate probed with 10^{-4} M fluoranthene. Inset shows the changes of the Raman band intensity centered at 559 cm^{-1}.

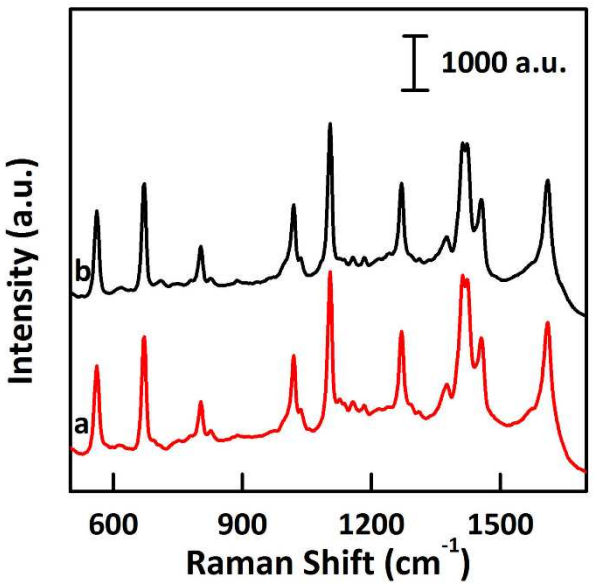

Fig. 5 Long-term stability of the substrate. SERS spectra of 10^{-4} M fluoranthene obtained from (a) the freshly prepared substrate and (b) the substrate immersed in the analyte solution for 3 days.

The inset image of Fig. 4A showed the relative standard deviation (RSD) of the peak intensity at 559 cm^{-1} was 5.06%, indicating that the substrate had a good temporal stability under laser irradiation. As illustrated in Fig. 4B, the SERS signals achieved from sixteen points randomly chosen on the gold nanostructures were very similar, indicating that the uniformity of the substrate was fairly good. The inset image of Fig. 4B showed the RSD of the intensity was 9.0% from sixteen different points. Meanwhile, as shown in Fig. 5, the duration stability of the substrate in an aqueous solution was also investigated by comparing the SERS spectrum of the freshly prepared and aged substrate. It was observed that neither the overall shape nor the SERS intensity had any significant change after immersion in the fluoranthene solution for 3 days, indicating the good stability of the as-prepared substrate. Therefore, the gold nanostructures had indeed shown stability for the SERS measurements besides good uniformity.

Other than the uniformity and stability, an ideal SERS sensor would also has good reproducibility. In this work, the reproducibility of the SERS-active substrate was evaluated by repeating the process of adsorption and elution. The SERS-active substrate was cyclic immersed in the solution of fluoranthene and ethanol, and then their corresponding SERS spectra were recorded (see Fig. S5). It was clear that neither the positions nor the height of the characteristic peaks of fluoranthene significantly vary after five cycles. The above results illustrated the substrate had good temporal stability, uniformity, and reproducibility.

Qualitative and quantitative SERS detection of PTS

To obtain qualitative analysis of PTS, SERS-active substrate was exposed to each PTS solution. The data points were recorded from three randomly selected positions on the substrate. The SERS spectra and the proposed peak assignments of fluoranthene, BDE-15 and PCB-15, Raman spectra of the corresponding solid compounds and their chemical structures were displayed in Fig. S6, Table S1 and Fig. S7, respectively. It

RSC Advances Accepted Manuscript

This journal is © The Royal Society of Chemistry [year]

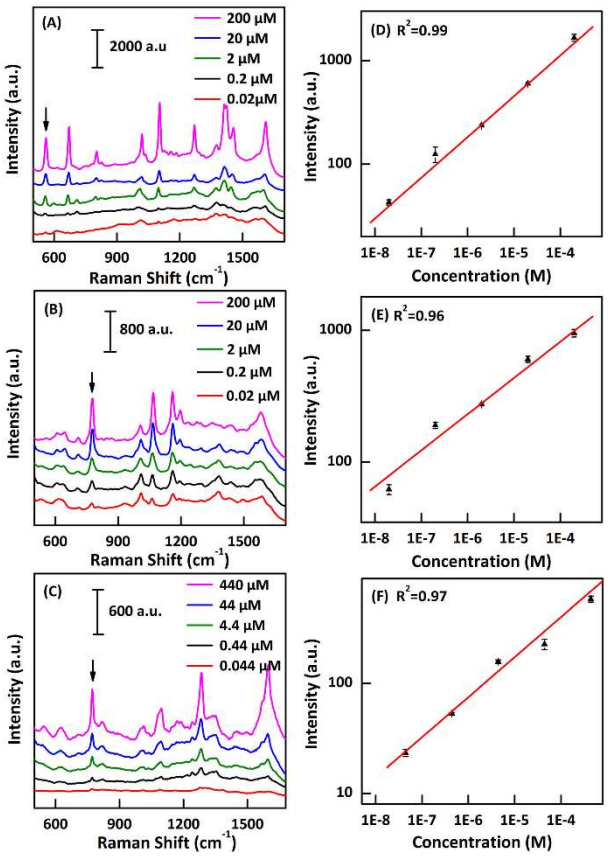

Fig. 6 (Left) SERS spectra of three PTS at different concentrations (A) fluoranthene (B) BDE-15 (C) PCB-15. (Right) log–log plots for (D) fluoranthene at 559 cm^{-1}, (E) BDE-15 at 776 cm^{-1}, (F) PCB-15 at 772 cm^{-1}. Each data point represents the average value from three SERS spectra. Error bars show the standard deviations

was noted that the SERS spectra of PTS were comparable to the Raman spectra, suggesting that the PTS had adsorbed onto the substrate surface. Quantitative SERS analysis of PTS was also carried out. Distinct SERS spectra of PTS in different concentrations were collected as shown in Fig. 6. As seen in Fig. 6A, the intensity of the peaks increased with the increasing of the fluoranthene concentration, and the peak at 559 cm^{-1} could be observed as low as 0.02 μM. The log-log plot of the intensity at 559 cm^{-1} to fluoranthene concentration yielded a good linear relationship (shown in Fig. 6D). Additionally, the limit of detection (LOD) was determined to be about 6.7 nM. The three PTS all had similar quantitative results.

SERS intensity can be described as follows.[40]

$$I_{SERS} = NI_L \left|A(\nu_L)\right|^2 \left|A(\nu_S)\right|^2 \sigma_{ads}^R \quad (1)$$

where I_{SERS} represents the intensity of SERS signal, N represents the molecular number participated in the SERS process, I_L is the excitation intensity, $A(\nu_L)$ and $A(\nu_S)$ are, respectively, excitation and scattered field enhancement factors. σ_{ads}^R is the increased Raman cross section of the adsorbed molecule as compared to that in a ''normal'' Raman experiment σ^R. I_L, $A(\nu_L)$, $A(\nu_S)$, and σ_{ads}^R could be considered as constants in an established quantitative detection experiment.

On the other hand, the adsorption of the analyte on the substrate at equilibrium could generally be well-described using the Freundlich equation.[41]

$$N = kc^{\frac{1}{n}} \quad (2)$$

where c is the equilibrium concentration of PTS in the liquid matrix. *k* and *n* are constants for a given adsorbate and adsorbent at a particular temperature.

Thus, equation (1) can be written using the following format.[42]

$$I_{SERS} = aN = akc^{\frac{1}{n}} = Kc^{\frac{1}{n}} \quad (3)$$

where a and *K* are constants including all other parameters and are not related to PTS concentration.

The equation (3) could be expressed as follows.

$$\log I_{SERS} = \log K + \frac{1}{n}\log c \quad (4)$$

As seen from equation (4), it is reasonable that the good linear relationship of the log-log plot for SERS intensity to analyte concentration could be exhibited.

The above results indicated that the substrate had high sensitivity for detecting hydrophobic PTS using SERS measurement mainly attributed to two aspects. Firstly, the morphology of gold nanostructures could be responsible for SERS efficiency. Compared to the bare gold electrode, the modified electrode possessed more SERS "hot spots" due to the robust surface morphology, which resulted in a Raman enhancement when PTS molecules were adsorbed on the substrate. Secondly, it was attributed to the hydrophobicity of the as-obtained gold nanostructures which improved the ability of the substrates to enrich hydrophobic PTS compounds. Fluoranthene, BDE-15 and PCB-15 were selected as target compounds and the high octanol-water partition coefficient (K_{ow}) values indicated their hydrophobic property (see Table S2). As a result, the experimental results further confirmed that the remarkable enhancement of Raman spectroscopy for detecting PTS was ascribed to the surface morphology and the hydrophobicity of the gold nanostructures. The as-prepared substrate had a comparable enhancement factor, detection limit and linear range compared with other substrates for SERS detection, which were summarized in Table S3.

Detection of fluoranthene in simulated water samples

In order to investigate the capability of the as-fabricated substrate for SERS detection of PTS in the real-world water, fluoranthene was chosen as probe molecule, dissolved in real spring water. The spring water was obtained from Black Tiger Spring (Jinan, China) and filtered through a 0.22 μm syringe filter before use. The samples were prepared by adding target analytes into the spring water samples. The SERS spectra of fluoranthene at different concentrations were shown in Fig. S8. Obviously, the intensity of the SERS peak at 559 cm^{-1} increased with increasing the concentration of fluoranthene over the concentration range of 0.2 μM to 200 μM. As displayed in Fig. S8, SERS spectra of the simulated water samples in the presence and absence of

RSC Advances Accepted Manuscript

Cite this: DOI: 10.1039/c0xx00000x

www.rsc.org/xxxxxx

ARTICLE TYPE

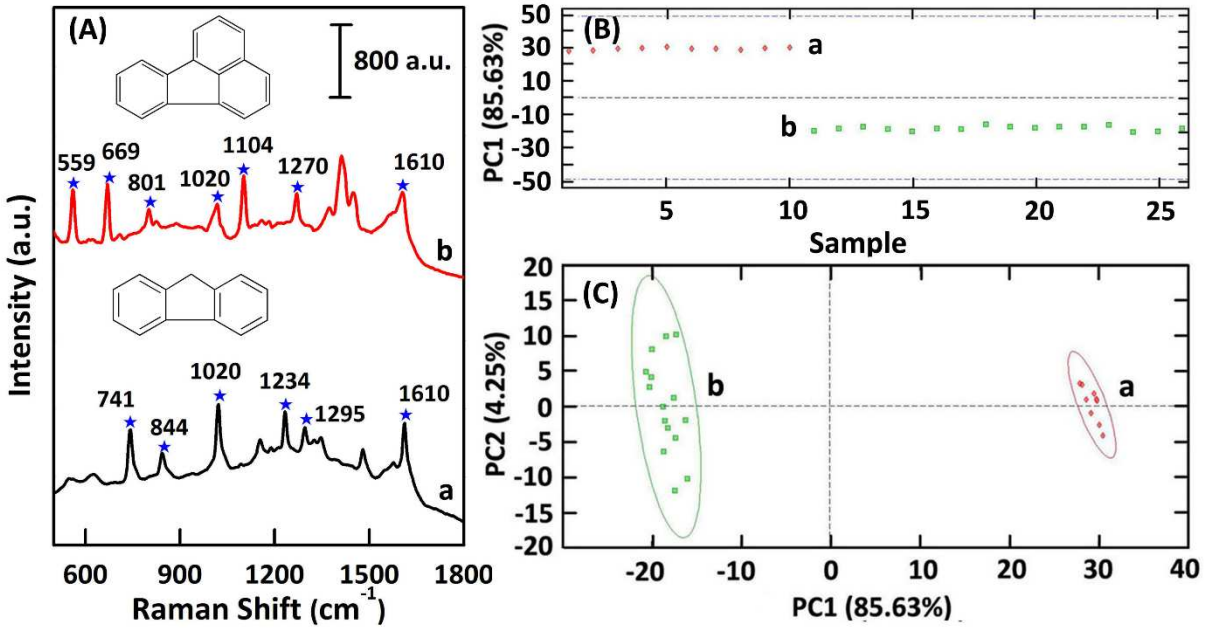

Fig. 7 (A) SERS spectra of (a) fluorene and (b) fluoranthene probed by using the substrate. (B) PCA plots (PC1 vs sample) of the recorded SERS spectra of fluorene and fluoranthene. (C) PCA plots (PC1 vs PC2) for fluorene and fluoranthene. The SERS spectra were handled based on first-derivative spectra in the 500-1600 cm^{-1} range. Each cluster ring is a two-dimensional standard deviation.

fluoranthene were obtained. It was demonstrated that the natural organic matter (NOM) in water samples would not interfere with the SERS detection of fluoranthene and fluoranthene contents were below the detection limits. The results of recovery for spring water samples of the proposed method were obtained and compared with those of chromatography. The analytical performances are summarized in Table S4. These results imply that the as-fabricated substrate can be an excellent candidate for fast and sensitive monitoring PTS in real water samples.

Principal component analysis of fluoranthene and fluorene

To gain a better understanding of analytes with similar characteristics and SERS spectra, principle component analysis (PCA) was applied to develop mathematical models. Fluoranthene and fluorene were chosen as model molecules (Fig. 7). The multivariate data analysis was carried out with MatLab software subroutines. PCA was used to dramatically reduce the dimensionality of the large spectral arrays, maximize the spectral variances resulting from these input data arrays. The differences between the SERS spectra of fluoranthene and fluorene were found in the higher principal components (Fig. 7B). The first principal component, known as PC1, accounted for the most variance in the dataset, and as a result it was near the average of all the spectra. As shown in Fig. 7C, two different clusters formed indicating that the PCA method was able to discriminate and to detect fluoranthene and fluorene with similar SERS spectra. The PCA analysis of the SERS spectra results in clusters, which demonstrates the enhanced specificity as well as sensitivity obtained from the SERS approach.

Conclusions

In summary, hydrophobic gold nanostructures fabricated by an electrochemical deposition process were served as effective SERS substrates to monitor PTS, analytes having weak affinity to noble metal surface. Acceptable data could be acquired from the portable Raman spectrometer within just a few seconds. The contact angle changed from 77° to 123° with extension of the deposition time, indicating the wetting property of the surface changed from hydrophilic to hydrophobic, which is consistent with the Cassie equation. Owing to the hydrophobicity, the as-obtained substrates exhibited strong affinity to hydrophobic contaminants. The enhancement factor (EF) values for fluoranthene, 4, 4′-dibromodiphenyl ether (BDE-15) and 4, 4′-dichlorobiphenyl (PCB-15) were 1.5×10^4, 2.6×10^4, 1.2×10^4, respectively. According to the Freundlich equation, the log-log plot of the SERS intensity of PTS to its concentration exhibits a good linear relationship. Quantitative detection of fluoranthene, BDE-15 and PCB-15 was achieved with the detection limits of 6.7 nM, 2.6 nM and 5.3 nM, respectively. The high temporal stability and uniformity mean that the SERS-active substrates very suitable for environmental monitoring. SERS detection of PTS in spring water was realized. The effective substrate provides a rapid and sensitive platform for SERS detection of

RSC Advances Accepted Manuscript

hydrophobic contaminants in the environment.

Acknowledgments

We are grateful for financial support from National Basic Research Program of China (973 Program 2013CB934301), National Natural Science Foundation of China (NSFC 21377068, 21075077), Shandong Provincial Natural Science Foundation for Distinguished Young Scholar (2010JQE27013), Shandong Provincial Natural Science Foundation (ZR2014BM033), Independent Innovation Foundation of Shandong University (IIFSDU- 2012JC027).

Notes and references

Key Laboratory for Colloid & Interface Chemistry of Education Ministry, Department of Chemistry, Shandong University, Jinan Shandong, 250100, P. R. China. E-mail: jhzhan@sdu.edu.cn

† Electronic Supplementary Information (ESI) available: [details of any supplementary information available should be included here]. See DOI: 10.1039/b000000x/

1 A. Meimaridou, K. Kalachova, W. Shelver, M. Franek, J. Pulkrabova, W. Haassnoot and M. Nielen, *Anal. Chem.,* 2011, **83**, 8696-8702.
2 J. Tan, Q. Q. Li, A. Loganath, Y. S. Chong, M. Xiao and J. P. Obbard, *Environ. Sci. Technol.,* 2008, **42**, 2681-2687.
3 J. W. Xu, J. J. Du, C. Y. Jing, Y. L. Zhang and J. L. Cui, *ACS Appl. Mater. Interfaces,* 2014, **6**, 6891-6897.
4 K.-L. Ho, M. B. Murphy, Y. Wan, B. M.-W. Fong, S. Tam, J. P. Giesy, K. S.-Y. Leung, M. H.-W. Lam, *Anal. Chem.,* 2012, **84**, 9881-9888.
5 M. Rahimi and E. Noroozian, *Anal. Chim. Acta,* 2014, 836, 45–52.
6 M. P. Zakaria, H. Takada, H. Tsutsumi, K. Ohno, J. Hamada, E. Kouno and H. Kumata, *Environ. Sci. Technol.,* 2002, **36**, 1907–1918.
7 T. Z. Zheng, T. R. Holford, J. Tessari, S. T. Mayne, P. H. Owens, B. Ward, D. Carter, P. Boyle, R. Dubrow, S. Archibeque-Engle and S. H. Zahm, *Am. J. Epidemiol.,* 2000, **152**, 50–58.
8 P. Serôdio and J. M. F. Nogueira, *Anal. Chim. Acta,* 2004, **517**, 21-32.
9 L. Debrauwer, A. Riu and M. Covaci, *J. Chromatogr. A,* 2005, **1082**, 98-109.
10 P. Braun, M. Moeder, S. Schrader, P. Popp, P. Kuschk and W. Engewald, *J. Chromatogr. A,* 2003, **988**, 41-51.
11 S. Ozcan, A. Tor and M. E. Aydin, *Anal. Chim. Acta,* 2009, **647**, 182-188.
12 J. F. Focant, J. W. Cochran, J. M. D. Dimandja, E. DePauw, A. Sjodin, W. E. Turner and D. G. Patterson, *Analyst,* 2004, **129**, 331-336.
13 Y. Zhu, K. Morisato, W. Y. Li, K. Kanamori and K. Nakanishi, *ACS Appl. Mater. Interfaces,* 2013, **5**, 2118-2125.
14 S. S. R. Dasary, A. K. Singh, D. Senapati, H. T. Yu and P. C. Ray, *J. Am. Chem. Soc.,* 2009, **131**, 13806-13812.
15 W. T. Lu, A. K. Singh, S. A. Khan, D. Senapati, H. T. Yu and P. C. Ray, *J. Am. Chem. Soc.,* 2010, **132**, 18103-18114.
16 C. H. Zhu, G. W. Meng, Q. Huang and Z. L. Huang, *J. Hazard. Mater.,* 2012, **211**, 389-390.
17 D. Li, D. W. Li, J. S. Fossey and Y. T. Long, *Anal. Chem.,* 2010, **82**, 9299-9305.
18 K. L. Rule and P. Vikesland, *Environ. Sci. Technol.,* 2009, **43**, 1147-1152.
19 X. Y. Zhang, M. A. Young, O. Lyandres and R. P. Van Duyne, *J. Am. Chem. Soc.,* 2005, **127**, 4484-4489.
20 X. J. Liu, L. Y. Cao, W. Song, K. L. Ai and L. H. Lu, *ACS Appl. Mater. Interfaces,* 2011, **3**, 2944–2952.
21 J. F. Li, Y. F. Huang, Y. Ding, Z. L. Yang, S. B. Li, X. S. Zhou, F. R. Fan, W. Zhang, Z. Y. Zhou, D. Y. Wu, B. Ren, Z. L. Wang, Z. Q. Tian, *Nature,* 2010, **464**, 392-395.
22 L. Guerrini, J. V. Garcia-Ramos, C. Domingo and S. Sanchez-Cortes, *Anal. Chem.,* 2009, **81**, 953-960.
23 X. M. Qian and S. M. Nie, *Chem. Soc. Rev.,* 2008, **37**, 912-920.
24 R. A. Halvorson and P. J. Vikesland, *Environ. Sci. Technol.,* 2010, **44**, 7749-7755.
25 L. Guerrini and D. Graham, *Chem. Soc. Rev.,* 2012, **41**, 7085-7107.
26 E. C. Le Ru and P. G. Etchegoin, *Principles of Surface-Enhanced Raman Spectroscopy*, Elsevier, Amsterdam, 2009.
27 D. Huang, X. T. Bai and L. Q. Zheng, *J. Phys. Chem. C,* 2011, **115**, 14641-14647.
28 M. Pan, H. Sun, J. W. Lim, S. R. Bakaul, Y. Zeng, S. X. Xing, T. Wu, Q. Y. Yan and H. Y. Chen, *Chem. Commun.,* 2012, **48**, 1440-1442.
29 X. L. Tang, P. Jiang, G. L. Ge, M. Tsuji, S. S. Xie and Y. J. Guo, *Langmuir,* 2008, **24**, 1763-1768.
30 J. Zhang, L. Meng, D. Zhao, Z. Fei, Q. Lu and P. J. Dyson, *Langmuir,* 2008, **24**, 2699-2704.
31 X. L. Xu, J. B. Jia, X. R.Yang and S. J. Dong, *Langmuir,* 2010, **26**, 7627-7631.
32 T. H. Lin, C. W. Lin, H. H. Liu, J. T. Sheu and W. H. Hung, *Chem. Commun.,* 2011, **47**, 2044-2046.
33 M. Shanthil, R. Thomas, R. S. Swathi and G. K. Thomas, *J. Phys. Chem. Lett.,* 2012, **3**, 1459-1464.
34 J. P. Yuan, Y. C. Lai, J. L. Duan, Q. Q. Zhao and J. H. Zhan, *J. Colloid Interface Sci.,* 2012, **365**, 122-126.
35 C. H. Zhu, G. W. Meng, Q. Huang, Z. B. Li, Z. L. Huang, M. L. Wang and J. P. Yuan, *J. Mater. Chem.,* 2012, **22**, 2271-2278.
36 Y. Xie, X. Wang, X. Han, W. Song, W. Ruan, J. Liu, B. Zhao and Y. Ozaki, *J. Raman Spectrosc.,* 2011, **42**, 945–950.
37 Y. C. Lai, J. C. Cui, X. H. Jiang, S. Zhu and J. H. Zhan, *Analyst,* 2013, **138**, 2598-2603.
38 X. H. Jiang, Y. C. Lai, M. Yang, H. Yang, W. Jiang and J. H. Zhan, *Analyst,* 2012, **137**, 3995-4000.
39 X. H. Jiang, Y. C. Lai, W. Wang, W. Jiang and J. H. Zhan, *Talanta,* 2013, **116**, 14-17.
40 K. Kneipp, H. Kneipp, I. Itzkan, R. R. Dasari and M. S. Feld, *Chem. Rev.,* 1999, **99**, 2957-2975.
41 A. Proctor and J. F. Toro-Vazquez, *J. Am. Oil Chem. Soc.,* 1996, **73**, 1627-1633.
42 X. H. Jiang, M. Yang, Y. J. Meng, W. Jiang and J. H. Zhan, *ACS Appl. Mater. Interfaces,* 2013, **5**, 6902-6908.

RSC Advances Accepted Manuscript